

Geometric Structures and Magnetic Interactions in Small Chromium Oxide Clusters

Le Nhan Pham,^{†,‡,§} Pieterjan Claes,[¶] Peter Lievens,[¶] Ling Jiang,^{§,||} Torsten Wende,[§]
Knut R. Asmis,[§] Minh Tho Nguyen,^{*,†} and Ewald Janssens^{*,¶}

[†]Department of Chemistry, KU Leuven, Celestijnenlaan 200F, B-3001 Leuven, Belgium

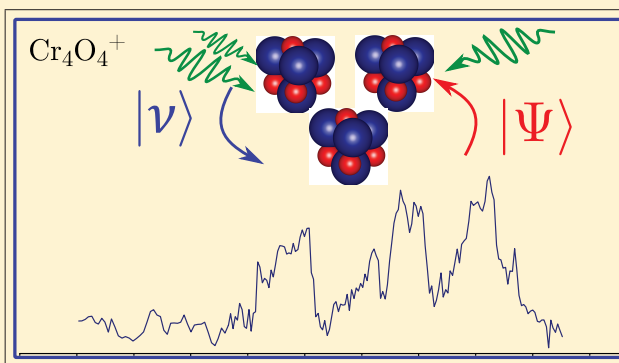
[‡]Department of Chemistry, The University of Dalat, 670000 Dalat, Vietnam

[¶]Laboratory of Solid State Physics and Magnetism and Department of Physics and Astronomy, KU Leuven, Celestijnenlaan 200D, B-3001 Leuven, Belgium

[§]Wilhelm-Ostwald-Institute for Physical and Theoretical Chemistry, University of Leipzig, Linnestrasse 2, D-04103 Leipzig, Germany

Supporting Information

ABSTRACT: The physical and chemical properties of transition metal oxide particles result from the subtle interplay between atomic ordering and electronic structure, the latter being determined by a complex interaction between the partially filled d subshell of the transition metal atoms and the oxygen 2p orbitals. In this article, the geometric ground state structures of several experimentally synthesized cationic chromium oxide clusters Cr_mO_n^+ ($m = 2, 3, 4; n \leq m$) are characterized through infrared photodissociation spectroscopy on cluster-rare gas atom complexes in combination with quantum chemical calculations. Computational analysis of the electronic and magnetic properties of the identified isomers demonstrated that the magnetic configuration of the clusters varies with the size and oxidation state. Superexchange interaction causes ferromagnetic coupling in Cr_2O_2^+ and Cr_3O_3^+ , while 3d–3d bonding-like interaction between two chromium atoms underlies ferrimagnetic behavior in Cr_3O^+ , Cr_3O_2^+ , and Cr_4O_4^+ . The highest possible total magnetic moments are obtained in suboxides that have Cr–O–Cr bridges with a unique oxygen atom between each pair of Cr atoms. The addition of more oxygen atoms enhances the delocalization of the Cr 3d electrons and reduces the magnetic moment.



INTRODUCTION

Bulk chromium is an antiferromagnetic material at room temperature (its Néel temperature is about 308 K) and behaves paramagnetically at higher temperatures.¹ The chromium atom has, in the ground state, six unpaired electrons in its 3d and 4s orbitals. In the smallest possible cluster of chromium atoms, the Cr_2 dimer, the total magnetic moment is zero as a result of antiferromagnetic coupling of the local moments.^{2–4} Interestingly, the Cr–Cr bond length is significantly increased and the local moments at the two chromium sites couple ferromagnetically if one electron is removed resulting in a high-spin ground state ($^1\Sigma$) for Cr_2^+ .⁴ Triatomic and other small odd sized chromium clusters are subject to antiferromagnetic frustration.^{5,6} In a recent theoretical study, an energetic competition between low and high spin states ($S = 1$ and $S = 6$) was found in Cr_4 as a result of the highly correlated electron behavior.⁷

Magnetic interactions in pure chromium clusters can be altered by addition of oxygen atoms. Superexchange through bridging oxygen atoms induces a ferromagnetic coupling

between the local moments on the two Cr atoms in $\text{Cr}_2\text{O}_n^{-/0}$ ($n = 1–3$).^{8,9} Further addition of oxygen reduces, and even quenches, total magnetic moments of the dichromium clusters (Cr_2O_n , $n = 4–14$).^{10,11} A similar observation was made for larger clusters; the local magnetic moments of chromium atoms are quenched in clusters with a high oxygen concentration, such as Cr_4O_{10} and $(\text{CrO}_3)_n$ ($n = 1–5$).^{12,13} Such quenching happens because all chromium valence electrons are involved in chemical bonds with oxygen atoms. In suboxide clusters, such as $\text{Cr}_3\text{O}_n^{+/0}$ ($n = 0–3$), the magnetic interactions are controlled by the amount of oxygen.⁵ Besides the composition (chromium to oxygen atomic ratio), also the precise geometry of the cluster is important for the magnetic interaction. It was, for example, found that Cr_nO_2 ($n = 2–5$) clusters of the same size but with a different geometric structure can have different magnetic properties and

Received: October 15, 2018

Revised: November 10, 2018

Published: November 13, 2018

interactions.^{14,15} Similar findings were reported for iron oxide clusters. For example, different magnetic states were predicted as lowest energy configuration of the neutral Fe_4O_6 , although these isomers have similar geometries (T_d versus slightly distorted T_d symmetry), including a ferromagnetic state with a magnetic moment of $20 \mu_B$,¹⁶ a ferrimagnetic $10 \mu_B$ state,¹⁷ and most recently a singlet state ($^1A_2, C_{2v}$).^{18,19} Therefore, it is important to identify the geometry of clusters produced in the experiment before assessing their magnetic ground state configurations. The cluster geometry can be accurately obtained from infrared photodissociation (IRPD) spectroscopy experiments on cluster–rare gas atom complexes. The detachment of the rare gas atoms is detected mass spectrometrically and signals resonant absorption of infrared photons. This spectroscopic technique, in combination with density functional theory (DFT) calculations, has been proven a powerful technique to identify the geometries of small metal oxide clusters.^{18,20–24}

To fully understand the interplay between chemical compositions, geometric arrangements, and magnetic properties of small chromium oxide clusters, we synthesized a series of cationic Cr_mO_n^+ ($m = 2, 3, 4; n \leq m$) clusters and studied them by a combination of infrared spectroscopy and quantum chemical calculations. Several quantum chemical methods were employed to locate ground-state and low-lying structures of the synthesized clusters. The magnetic interactions between and/or among local sites were studied. The evolution of magnetic moments through chemical control is discussed.

EXPERIMENTAL METHODS

The experiments were carried out using a molecular beam setup consisting of a cluster source, an ion guide, a mass filter, an ion trap, and a time-of-flight mass spectrometer.²⁵ This setup was temporarily installed at the Free Electron Laser for Infrared eXperiments (FELIX) facility (The Netherlands).²⁶ The chromium oxide clusters were prepared by a pulsed laser vaporization source operated at 10 Hz.^{20,27} The 2nd harmonic of a Nd:YAG laser is focused on a metallic Cr plate and creates a plasma, which is entrained in a pulse of 1% O_2 seeded in He carrier gas and expanded through a clustering channel. The chromium-oxide cluster beam is collimated and thermalized to room temperature by collisions with Ar atoms in a radio frequency (RF) decapole ion guide and mass-selected by a quadrupole mass filter. Mass-selected cationic clusters are accumulated in a ring electrode ion trap. To allow for continuous ion loading, ion thermalization, and cluster-rare gas (He, Ne) complex formation, the trap is continuously filled with a buffer gas of either pure He (for Cr_3O^+ and Cr_3O_2^+) or a mixture of 0.125% Ne in He (for Cr_2O_2^+ , Cr_3O_3^+ , and Cr_4O_4^+) at ion trap temperatures in the range of 20–35 K. After filling the trap for 98 ms, all ions are extracted and focused both temporally and spatially into the center of the extraction region of an orthogonally mounted linear time-of-flight (TOF) mass spectrometer. Here, the ion packet can be irradiated with the IR laser pulse. The absorption of a few and often only a single IR photon(s) by the weakly bound cluster-rare gas ionic complex is sufficient for vibrational predissociation and loss of the rare gas messenger. Scanning the wavelength of the excitation laser light provides the IRPD spectra, which are obtained in the difference mode of operation (laser on-laser off) and recorded by monitoring all ion intensities simultaneously. The infrared free electron laser FELIX is operated in the 400–750 cm^{-1} spectral range at a

repetition rate of 5 Hz, a bandwidth of 0.2% root-mean-square of the central wavelength and an average pulse energy of 10 mJ.

COMPUTATIONAL METHODS

The CALYPSO²⁸ tool was used to generate large numbers of initial structures at relatively low computational levels (B3LYP/3-21G and BP86/3-21G). The generated low-lying energetic structures were subsequently reoptimized with the larger cc-pVTZ basis set.^{29,30} Different spin multiplicities were tested for all structural isomers. Various density functionals (B3LYP,^{31–33} B3P86,^{33,34} B3PW91,³³ BP86,^{32,34} TPSS,³⁵ TPSSh, and M06L³⁶) have been tested to ensure reliability of the obtained results. In addition, for Cr_2O_2^+ the restricted active space followed by second-order perturbation treatment (RASSCF/RASPT2) and coupled cluster (CCSD(T)-F12) methods have been used as benchmark for the DFT calculations. More details about these computational processes are provided in the [Supporting Information](#). Throughout the calculation process, the TPSS functional appears to be excellent in vibrational simulations of the obtained clusters in comparison to the other used functionals; therefore the simulated spectra from this functional are used as the basis for 4 out of 5 spectral assignments in this work. The B3P86 functional was used for Cr_2O_2^+ , since the IR spectrum of its $^8\text{B}_{1u}$ state could not be assessed at the TPSS level (see [Supporting Information](#) for details). DFT energies were corrected for zero point energies (ZPEs) at corresponding levels of theory, unless otherwise stated. The harmonic vibrational frequencies of the ground and first excited states were analytically obtained after DFT optimizations. If not explicitly specified in the text, harmonic vibrational frequencies were calculated with the Gaussian 09 program.³⁷ The empirical dispersion correction GD3³⁸ (for supported functionals) for optimizations and spectral simulations was taken into account.

RESULTS AND DISCUSSION

Structural Assignments. Starting from the simplest synthesized cluster Cr_2O_2^+ , two clear bands around 610 and 720 cm^{-1} were observed from the experimental IRPD spectrum of the $\text{Cr}_2\text{O}_2^+\cdot\text{Ne}$ complex. The ground, first excited states and other low-lying ones of Cr_2O_2^+ are listed in Table S1 of the [Supporting Information](#). At all considered levels of theory the $^8\text{B}_{1g}$ and $^8\text{B}_{1u}$ states are much lower in energy, so we just focus on these two states. Comparing the geometrical structures of the $^8\text{B}_{1g}$ ground and the $^8\text{B}_{1u}$ excited states, small differences are found. The Cr–O bond is 0.01 Å longer when Cr_2O_2^+ is stimulated from the $^8\text{B}_{1g}$ ground state to the $^8\text{B}_{1u}$ first excited state. The bonding angles $\widehat{\text{OCrO}}$ and $\widehat{\text{CrOCr}}$ also stretch and bend, respectively, 5 deg in comparison to the ones of the ground state. In terms of electronic structures, these two states differentiate from each other in the occupation of electrons in b_{1g} and b_{1u} orbitals. The leading configurations of these different electronic states are given in Table S2 of the [Supporting Information](#).

The difference in energy between the ground state $^8\text{B}_{1g}$ and first excited state $^8\text{B}_{1u}$ at the RASPT2 level is 0.38 eV. Assuming Maxwell–Boltzmann statistics, occupancy of an excited state at +0.38 eV would be small. However, besides uncertainty on the calculated relative energy of the excited state, also the attachment of messenger rare gases may affect the energy differences between isomers. Because of short-

comings of the implementation of the RASPT2 calculational technique, the effect of rare gas messenger atoms on the excited states of Cr_2O_2^+ cannot be examined precisely. Taking into account the computational uncertainty of RASPT2 and other quantum chemical methods, the differences in geometrical structures of the ground and first excited states are insignificant, and it is well possible that both the ground and first excited state are populated in the experiment.

The experimental IRPD and simulated IR spectra of the Cr_2O_2^+ cluster are presented in Figure 1. Although the TPSS

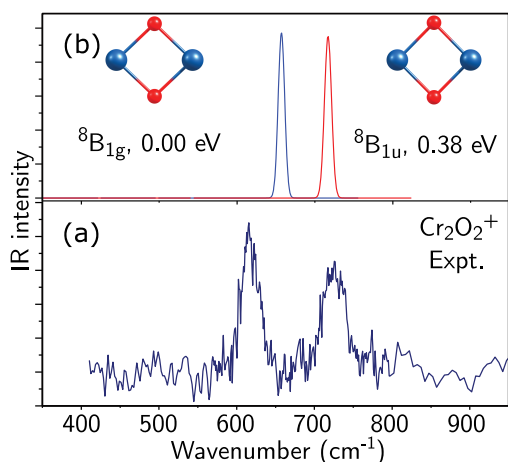


Figure 1. (a) Experimental IRPD spectra and (b) simulated harmonic IR spectra of Cr_2O_2^+ . The simulated spectrum of the ${}^8\text{B}_{1g}$ ground state is presented by the blue line and the spectrum of the ${}^8\text{B}_{1u}$ excited state by the red line. The geometries of the lowest-lying states are shown as insets.

functional is used for simulating the vibrational spectra of most clusters studied in this work, the simulated IR spectrum of excited state ${}^8\text{B}_{1u}$ could not be accessed at this level; therefore, the simulated spectra of these two states at the B3P86 level are used in Figure 1b. The simulated IR spectrum in Figure 1b is consistent with those obtained for the same isomer using other

DFT functionals (TPSSH, B3PW91, B3P86, B3LYP, M06L, and BP86) (see Figure S9 of the Supporting Information). Note that the interaction of the cationic chromium oxide clusters with the rare gas messenger atoms (Ne and He) does not significantly affect the simulated IR spectra (see Figure S2 of the Supporting Information).

The simulated IR spectrum of the ground state (${}^8\text{B}_{1g}$) shows a single peak at around 630 cm^{-1} , which can only explain one of two experimental bands (Figure 1a). The first excited ${}^8\text{B}_{1u}$ state's simulated spectrum has a vibrational mode at around 700 cm^{-1} , 70 cm^{-1} above that of the ${}^8\text{B}_{1g}$ ground state (see Figure 1b). Their separation agrees reasonably well with the observed band separation of 90 cm^{-1} in the experimental spectrum. Therefore, both the ${}^8\text{B}_{1g}$ ground state and the ${}^8\text{B}_{1u}$ first excited state are proposed to be populated in the experiment. A similar observation has been made for $\text{Cr}_2\text{O}_2^{-/0,39}$.

Figure 2 presents experimental and simulated spectra of the Cr_3O_n^+ ($n = 1-3$) series. The IR spectrum of $\text{Cr}_3\text{O}^+\cdot\text{He}_2$ has a rather low signal-to-noise ratio, but shows a pronounced peak at 700 cm^{-1} (see Figure 2c). The lowest state is found to be ${}^6\text{A}'$ for a propeller-like isomer within the C_s symmetry. A D_{3h} isomer with a high spin ${}^{16}\text{A}'$ electronic state is identified as the first excited state. The predicted IR spectrum of the ${}^6\text{A}'$ ground state is in agreement with the experimental IRPD spectrum, i.e. the IR-active peak observed at 700 cm^{-1} is reproduced at 707 cm^{-1} . The IR spectrum of the first excited state does not match the experimental spectrum, because its intense mode is about 150 cm^{-1} red-shifted from the experimental feature.

The IRPD spectrum of Cr_3O_2^+ , measured on the $\text{Cr}_3\text{O}_2^+\cdot\text{He}$ complex, has three clear bands at $630, 680,$ and 725 cm^{-1} . The simulated IR spectra of the sextet ground and a 14-et first excited state (see Figure 2, parts d and e) were used to determine the experimentally populated structure of Cr_3O_2^+ . For the ${}^6\text{A}$ state state, the TPSS method reproduces the three main experimental infrared active vibrations. Simulated spectra of these isomers using other DFT functionals are similar and can be found in the Supporting Information (Figure S11). We note that calculated harmonic IR spectra are typically reliable

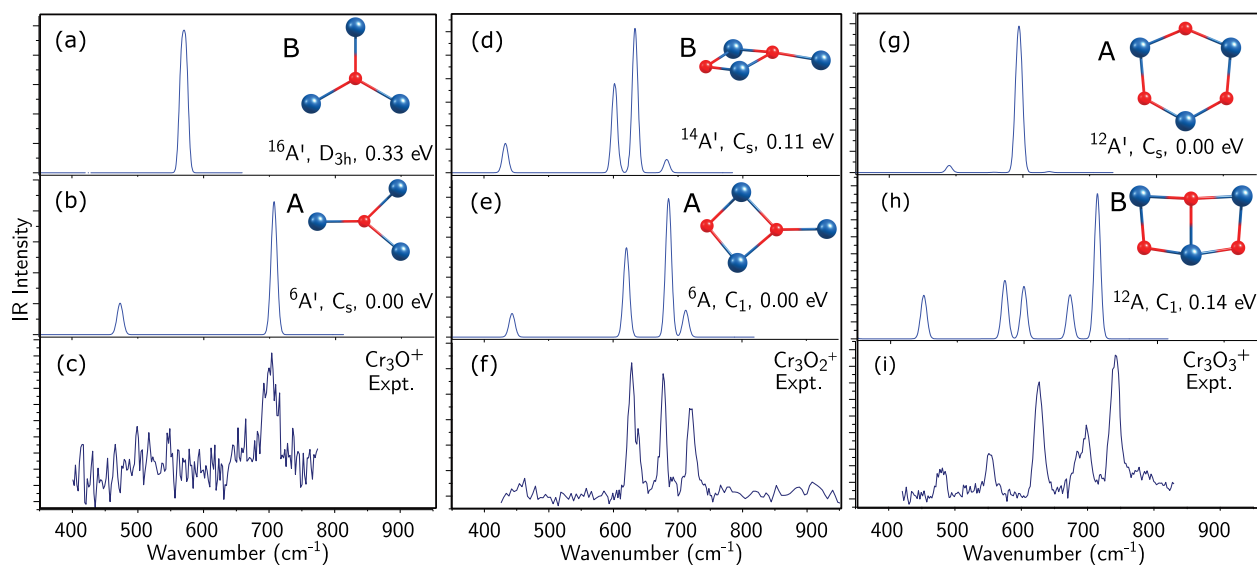


Figure 2. Experimental IRPD spectra and simulated harmonic IR spectra of Cr_3O^+ , Cr_3O_2^+ , and Cr_3O_3^+ . The geometries of lowest-lying states for each cluster are shown as insets.

to reproduce the number and the frequencies of the vibrational modes that are seen experimentally, but are less accurate for predicting the relative intensities of those modes. The main reasons for this are the multiple photon aspect and the statistical dissociation of the cluster-rare gas complexes in the experiment, which are not included in the computations. A detailed discussion of the consequences of those effects can be found in ref 40. So we conclude that the sextet state is likely the isomer that is observed in the experiment. However, the first excited state ${}^4A'$ is quite close to the ground state in terms of energy (+0.11 eV at the TPSS level), and its simulated spectrum is similar to the one of the 6A state. Therefore, both isomers may coexist in the experiment.

For $Cr_3O_3^+$ two isomers with a high spin 12-tet (noted as A and B in Figure 2, parts g and h, respectively) are energetically competitive. Although the calculated relative energy of isomer B (+0.14 eV) is slightly higher than that of isomer A, its simulated IR spectrum agrees much better with the experiment performed on the $Cr_3O_3^+ \cdot Ne$ complex with regard to the frequency of the modes and the number of peaks. We, therefore, assign the spectrum to isomer B. Note that the relative energy difference is comparable to the accuracy of the computational method. As reported in Table S6 of the Supporting Information, different hybrid and metaGGA functionals either predict isomer A (TPSS, B3LYP, B3PW91, TPSSH) or isomer B (M06L, B3P86) as most stable isomer with a maximal energy difference of 0.17 eV.

The IRPD spectrum of $Cr_4O_4^+$ (see Figure 3) shows several vibrational bands, which are grouped in three ranges: 550–

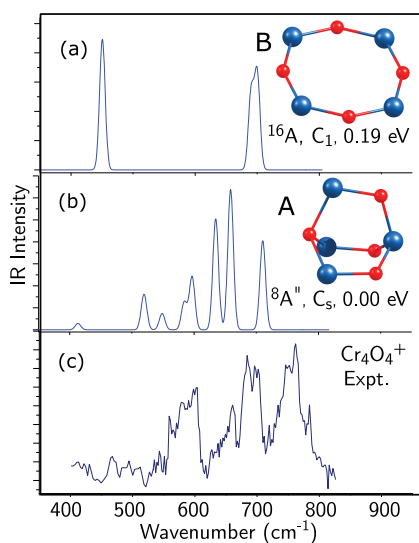


Figure 3. Experimental IRPD spectra and simulated harmonic IR spectra of $Cr_4O_4^+$. The geometries of the two most stable isomers are shown as insets.

600, 650–710, and 750–790 cm^{-1} . In the computational study, many different local minima were obtained for $Cr_4O_4^+$. Two structural motifs were found to be more stable: a cage-like structure (isomer A) and a ring-like structure (isomer B). Two most stable isomers of $Cr_4O_4^+$, their lowest energy electronic states, and corresponding simulated IR spectra are visualized in Figure 3. The simulated IR spectrum of isomer A in the octet state is in substantially better agreement with the experiment performed on the $Cr_4O_4^+ \cdot Ne$ complex, than that of isomer B. The only discrepancy is a redshift of the simulated spectrum by

40 cm^{-1} , particularly for the intense bands in the 670–760 cm^{-1} range. However, with the B3LYP, B3PW91 and B3P86 functional (see Figure S13 in the Supporting Information), the redshift for these bands is much smaller ($<10 cm^{-1}$). The IR spectrum of the cyclic isomer B only predicts two IR-active bands and cannot explain the more complex spectrum observed in the experiment.

From the above results, one can recognize that different structural motifs result in different IR spectra. In certain cases also similar structural motifs with a different spin state and thus different magnetic configurations can be distinguished by their IR spectra. This is the case for $Cr_4O_4^+$. Figure 4 presents four

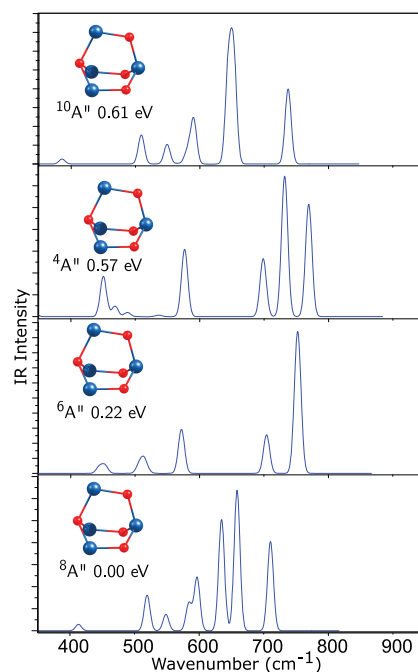


Figure 4. Simulated harmonic IR spectra of structural isomer A of $Cr_4O_4^+$ in four different spin states.

different spin configurations (quartet, sextet, octet, and decet) of structural isomer A of $Cr_4O_4^+$, with the octet spin state having the lowest energy. The simulated IR spectra of those different spin states are distinct from each other. This implies that the IRPD technique is, in this specific case, a suitable tool to not only probe the geometric structure but also spin configurations. This constitutes clear evidence of the direct relationship between the identification of vibrational spectra with the IRPD technique and magnetic properties.

Magnetic Properties. After assigning the geometric structures and the electronic states of the chromium oxide clusters by comparing the measured with simulated IR spectra, computations can be used to analyze the magnetic properties of the clusters. Local spin moments of individual atoms, which combine to give total spin magnetic moments of clusters, are graphically presented in Figure 5. Values of these local spin magnetic moments are given in Table 1. Also Cr_3^+ , $Cr_3O_4^+$, and $Cr_3O_5^+$ are added to the figure and the table. For these sizes, we only have computational results and no assignment of their structure based on the infrared spectra was performed. The spin magnetic configurations of the clusters can be divided into two groups: (i) clusters in which chromium spin moments are ferromagnetically coupled ($Cr_2O_2^+$, $Cr_3O_3^+$, $Cr_3O_4^+$, and

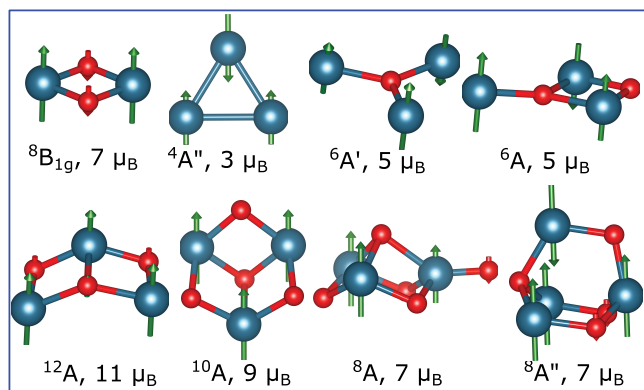


Figure 5. Structures of Cr_2O_2^+ , Cr_3O^+ , Cr_3O_2^+ , Cr_3O_3^+ , and Cr_4O_4^+ as assigned by comparison of simulated IR spectra with the experimental IRPD spectra. In addition, the structures of Cr_3^+ , Cr_3O_4^+ , and Cr_3O_5^+ , for which no IRPD data is available, are added to the figure. Spin magnetic moments of Cr_3^+ , Cr_3O_4^+ , and Cr_3O_5^+ were calculated from their energetically lowest geometry and electronic states. Chromium and oxygen atoms are represented by blue and red balls, respectively. Green (red) arrows indicate the orientation of the local spin magnetic moments ($>0.05 \mu_B$) on the chromium (oxygen) atoms.

Cr_3O_5^+) and (ii) clusters in which metallic spin moments are ferrimagnetically coupled (Cr_3^+ , Cr_3O^+ , Cr_3O_2^+ , and Cr_4O_4^+). In the ground-state structures of Cr_2O_2^+ , Cr_3O_3^+ , Cr_3O_4^+ , and Cr_3O_5^+ all spin magnetic moments of the chromium atoms are parallel, which leads to high values of 7, 11, 9, and $7 \mu_B$, respectively. In Cr_3^+ , Cr_3O^+ , Cr_3O_2^+ , and Cr_4O_4^+ the total spin magnetic moment is reduced compared to the maximal values, resulting in spin moments of 3, 5, 5, and $7 \mu_B$, respectively.

3d–3d bonding-formation and superexchange-type interactions were demonstrated to underlie the corresponding magnetic properties in pure chromium clusters (Cr_2^0 , $\text{Cr}_3^{+/0}$)^{2,41,42} and dichromium oxide clusters ($\text{Cr}_2\text{O}_2^{-/0}$, and $\text{Cr}_2\text{O}_3^{-/0}$)^{8,9,43}. In this work, we find small antiferromagnetic spin moments on the oxygen atoms in Cr_2O_2^+ and Cr_3O_3^+ . Coupling between the chromium and oxygen sites in these clusters occurs through the hybridization between Cr 3d and O 2p orbitals. Such an orbital interaction is known as superexchange, and it enhances the parallel spin coupling between chromium atoms.^{8,9,43} Figure 6 pictorially provides the total density of states (TDOS) and partial density of states (PDOS) of Cr_3O_3^+ and Cr_3O^+ . In the case of Cr_3O_3^+ , the PDOS (Figure 6c) reveals, particularly for the alpha occupied orbitals, strong hybridization between the chromium 3d and the oxygen 2p orbitals in the -15.0 to -9.0 eV range (-9.0 eV is the energy

of the HOMO). The Cr_3^+ , Cr_3O^+ , Cr_3O_2^+ , and Cr_4O_4^+ clusters disclose ferrimagnetic magnetic behavior, in which one of chromium atoms has its magnetic moment in the reverse direction of the others. By analyzing interaction between the two closest chromium atoms in the C_s isomer of Cr_3O^+ , bonding-like features are found between those two chromium atoms (see Figure S14). The 3d PDOS of the antiferromagnetically coupled chromium atoms of this cluster show energetic overlap between α and β 3d occupied orbitals in the -10 to -8.5 eV range (Figure 6d). Therefore, 3d–3d-like bonding between two closest chromium atoms causes an antiferromagnetic coupling of the local spin magnetic moments, similar as in the Cr_2 dimers.^{41,42} A similar bonding-type formation is believed to be present in Cr_3O_2^+ and Cr_4O_4^+ (see Figures S14 and S15), where the spin moment of one of the chromium atoms in antiparallel to the other ones.

Next, we investigate the effect of atom-by-atom oxygen addition to the geometry and magnetism of the Cr_3^+ metallic cluster. Figure 7 presents the magnetic evolution of Cr_3O_n^+ ($n = 0 - 5$). With the addition of oxygen atoms, the total magnetic moment increases from $n = 0$ ($3 \mu_B$) to $n = 3$ ($11 \mu_B$). Such a strong increase of the total magnetic moment implies that direct 3d–3d bonding-type interaction, which favors antiferromagnetic coupling, becomes weaker upon addition of oxygen atoms, reducing the 3d–3d interaction. The 3d–3d bonding-type formation is dominated by the superexchange interaction in Cr_3O_3^+ , leading to a high total spin magnetic moment ($11 \mu_B$). The total spin magnetic moment is gradually reduced if more oxygen atoms are added ($n = 4$ and $n = 5$). Finally, the magnetic moment is expected to be quenched, as was computationally found for the di-chromium oxides Cr_2O_n ¹¹ ($n \geq 6$). This result unravels how the oxygen concentration affects and controls the total magnetic properties of trichromium oxides.

Overall the evolution of the structures and the magnetic configurations with the oxygen concentration indicates that the highest magnetic moments, i.e. parallel alignment of the local Cr spin magnetic moments, are obtained in suboxides that have enough oxygen atoms to form Cr–O–Cr bridges with a unique O atom between each pair of Cr atoms. For Cr_3O_n^+ this occurs in Cr_3O_3^+ . In this cluster the superexchange interaction is maximized and occurs without strong reduction of the local magnetic moments on the involved Cr atom (see Table 1). Addition of more oxygen atoms (i.e., in Cr_3O_4^+ and Cr_3O_5^+) results in the formation of Cr–O bonds with individual Cr atoms and the delocalization of the Cr 3d electrons in Cr–O shared orbitals. Such capturing of unpaired Cr 3d electrons

Table 1. Total Spin Magnetic Moments of Clusters and Local Spin Magnetic Moments of Chromium and Oxygen Atoms^a

cluster	state	spin magnetic moment (μ_B)	local spin magnetic moment (μ_B)										
			Cr ₁	Cr ₂	Cr ₃	Cr ₄	O ₁	O ₂	O ₃	O ₄	O ₅		
Cr_2O_2^+	$^8\text{B}_{1g}$	7	+3.6	+3.6				−0.07	−0.07				
Cr_3^+	^4A	3	−4.5	+3.8	+3.8								
Cr_3O^+	$^6\text{A}'$	5	+4.6	−4.5	+4.9			−0.02					
Cr_3O_2^+	^6A	5	+4.9	+3.9	−3.7			−0.03	0.00				
Cr_3O_3^+	^{12}A	11	+3.1	+4.0	+4.0			−0.06	−0.06	+0.01			
Cr_3O_4^+	^{10}A	9	+3.0	+3.0	+3.0			−0.02	−0.02	−0.02	+0.06		
Cr_3O_5^+	^8A	7	+1.3	+2.9	+2.9			−0.12	−0.01	+0.02	+0.02	+0.05	
Cr_4O_4^+	$^8\text{A}''$	7	+3.8	−3.1	+3.8	+2.6		−0.08	−0.01	−0.08	+0.03		

^aAll values were calculated making use of natural bond orbital (NBO) analysis on the basis of the TPSS electron density.

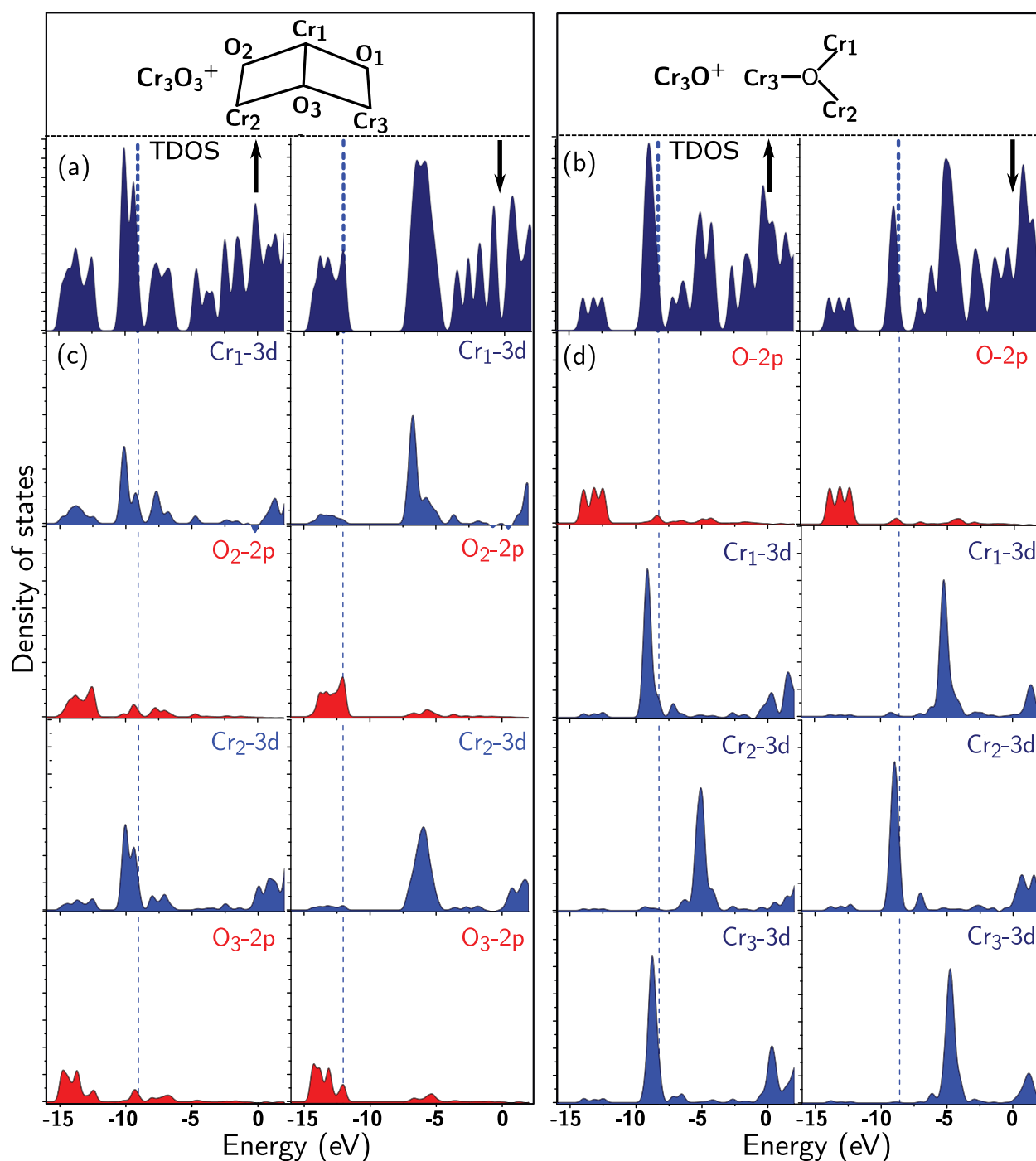


Figure 6. Total density of states (TDOS) and partial density of states (PDOS) of Cr_3O_3^+ (left part) and Cr_3O^+ (right part). For each part the left (right) side corresponds to alpha or up (beta or down) orbitals as indicated by the black arrows: (a) TDOS of Cr_3O_3^+ , (b) TDOS of Cr_3O^+ , (c) PDOS of Cr_3O_3^+ , and (d) PDOS of Cr_3O^+ . For PDOS, the projections in oxygen-2p (chromium-3d) orbitals are shown in red (blue). Atoms are numbered according to the structures shown in the insets. Vertical short dashed lines indicate the highest occupied alpha and beta orbitals.

reduces the Cr local magnetic moments. The observation of this magnetic configuration dependence on the oxygen concentration is empirical. An in-debt explanation may be the subject of follow-up studies.

CONCLUSION

In conclusion, several cationic chromium-rich oxides were synthesized and characterized through IR spectral characteristics. The magnetic states of these clusters were studied to reveal insights into their magnetic properties. Oxygen plays an

important role in controlling the magnetic configurations. Superexchange interaction through oxygen bridging sites causes ferromagnetic coupling of the chromium atoms in Cr_2O_2^+ and Cr_3O_3^+ . The ferrimagnetic behavior of Cr_3O^+ , Cr_3O_2^+ , and Cr_4O_4^+ is attributed to the bonds between the metal atoms, in which 3d orbitals of nearby chromium atoms directly interact with each other resulting in lower total spin magnetic moments. This study indicates that the highest possible total magnetic moments are obtained in suboxides with a comparable number of oxygen and chromium atoms

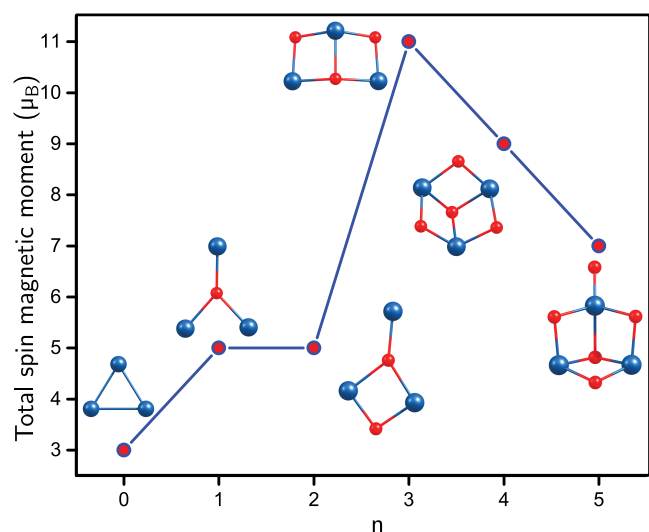


Figure 7. Evolution of the total spin magnetic moment for Cr_3O_n^+ ($n = 0 - 5$) clusters.

that have a unique oxygen atom in a single Cr–O–Cr bridge between each pair of Cr atoms. The addition of more oxygen atoms enhances the delocalization of the Cr 3d electrons and reduces the magnetic moment.

■ ASSOCIATED CONTENT

📄 Supporting Information

The Supporting Information is available free of charge on the ACS Publications website at DOI: 10.1021/acs.jpcc.8b10035.

Computational details for Cr_2O_2^+ ; geometrical structures and relative energies of different electronic states of Cr_2O_2^+ ; computational assessment of the influence of the rare gas messenger atoms on the IR spectra; structures of the lowest energy isomers of Cr_3O_m^+ ($m = 1-5$) and Cr_4O_4^+ ; calculated relative energies of Cr_3O_m^+ ($m = 1-5$) and Cr_4O_4^+ at different DFT levels; comparison of the IRPD spectra with simulated spectra at different DFT levels; AdNDP analysis of possible two-center bonding; and partial density of states of Cr_2O_2^+ , Cr_3O_2^+ , and Cr_4O_4^+ (PDF)

■ AUTHOR INFORMATION

Corresponding Authors

*(M.T.N.) E-mail: minh.nguyen@kuleuven.be.

*(E.J.) E-mail: ewald.janssens@kuleuven.be. Telephone: +32 16 32 72 07. Fax: +32 16 32 79 83.

ORCID

Le Nhan Pham: 0000-0001-9736-0747

Peter Lievens: 0000-0001-6570-0559

Ling Jiang: 0000-0002-8485-8893

Knut R. Asmis: 0000-0001-6297-5856

Minh Tho Nguyen: 0000-0002-3803-0569

Ewald Janssens: 0000-0002-5945-1194

Present Address

^{||}State Key Laboratory of Molecular Reaction Dynamics, Collaborative Innovation Center of Chemistry for Energy and Materials, Dalian Institute of Chemical Physics, Chinese Academy of Sciences, Dalian 116023, Liaoning, P. R. China

Notes

The authors declare no competing financial interest.

■ ACKNOWLEDGMENTS

This research has been supported by the Research Foundation - Flanders (FWO project G.0B41.15N) and by the KU Leuven Research Council (C14/18/073 and GOA program 2014). The authors are grateful to Dr. Liviu Ungur for his kind assistance with the MOLCAS program. The authors acknowledge support of the Stichting voor Fundamenteel Onderzoek der Materie (FOM) in providing beam time on FELIX and highly appreciate the skillful assistance of the FELIX staff.

■ REFERENCES

- (1) Fawcett, E. Spin-density-wave antiferromagnetism in chromium. *Rev. Mod. Phys.* **1988**, *60*, 209–283.
- (2) Bondybey, V.; English, J. Electronic structure and vibrational frequency of Cr_2 . *Chem. Phys. Lett.* **1983**, *94*, 443–447.
- (3) Riley, S. J.; Parks, E. K.; Pobo, L. G.; Wexler, S. The A←X transition in Cr_2 : Predissociation, isotope effects, and the 1–1 sequence band. *J. Chem. Phys.* **1983**, *79*, 2577–2582.
- (4) Zamudio-Bayer, V.; Hirsch, K.; Langenberg, A.; Niemeyer, M.; Vogel, M.; Ławicki, A.; Terasaki, A.; Lau, J. T.; von Issendorff, B. Maximum spin polarization in chromium dimer cations as demonstrated by x-ray magnetic circular dichroism spectroscopy. *Angew. Chem., Int. Ed.* **2015**, *54*, 4498–4501.
- (5) Janssens, E.; Hou, X. J.; Neukermans, S.; Wang, X.; Silverans, R. E.; Lievens, P.; Nguyen, M. T. The exchange coupling in Cr_3O_n ($n = 0 - 3$) clusters. *J. Phys. Chem. A* **2007**, *111*, 4150–4157.
- (6) Cheng, H.; Wang, L.-S. Dimer growth, structural transition, and antiferromagnetic ordering of small chromium clusters. *Phys. Rev. Lett.* **1996**, *77*, 51–54.
- (7) López-Estrada, O.; López-Olay, S.; Aburto, A.; Orgaz, E. Unexpected high spin polarization in Cr_4 cluster. *J. Phys. Chem. C* **2016**, *120*, 23892–23897.
- (8) Tono, K.; Terasaki, A.; Ohta, T.; Kondow, T. Chemical control of magnetism: Oxidation-induced ferromagnetic spin coupling in the chromium dimer evidenced by photoelectron spectroscopy. *Phys. Rev. Lett.* **2003**, *90*, 133402.
- (9) Tono, K.; Terasaki, A.; Ohta, T.; Kondow, T. Chemically induced ferromagnetic spin coupling: Electronic and geometric structures of chromium-oxide cluster anions, Cr_2O_n^- ($n = 1 - 3$), studied by photoelectron spectroscopy. *J. Chem. Phys.* **2003**, *119*, 11221–11227.
- (10) Reddy, B. V.; Khanna, S. N.; Ashman, C. Oscillatory magnetic coupling in Cr_2O_n ($n = 1 - 6$) clusters. *Phys. Rev. B: Condens. Matter Mater. Phys.* **2000**, *61*, 5797–5801.
- (11) Gutsev, G. L.; Bozhenko, K. V.; Gutsev, L. G.; Utenyshev, A. N.; Aldoshin, S. M. Transitions from stable to metastable states in the Cr_2O_n and Cr_2O_n^- series, $n = 1 - 14$. *J. Phys. Chem. A* **2017**, *121*, 845–854.
- (12) Li, S.; Zhai, H.-J.; Wang, L.-S.; Dixon, D. A. Structural and electronic properties of reduced transition metal oxide clusters, M_4O_{10} and $\text{M}_4\text{O}_{10}^-$ ($M = \text{Cr}, \text{W}$), from photoelectron spectroscopy and quantum chemical calculations. *J. Phys. Chem. A* **2012**, *116*, 5256–5271.
- (13) Zhai, H.-J.; Li, S.; Dixon, D. A.; Wang, L.-S. Probing the electronic and structural properties of chromium oxide clusters (CrO_3)_n[−] and (CrO_3)_n ($n = 1 - 5$): Photoelectron spectroscopy and density functional calculations. *J. Am. Chem. Soc.* **2008**, *130*, 5167–5177.
- (14) Pakiari, A. H.; Shariati, S. Geometry and electronic structure of ultrafine/nanoparticle chromium clusters (Cr_n , $n = 2-5$) and their interaction with oxygen (triplet) and ethylene molecules: A dft–nbo study. *Comput. Theor. Chem.* **2016**, *1084*, 169–178.
- (15) Shah, E. V.; Roy, D. R. Magnetic switching in Cr_x ($x = 2-8$) and its oxide cluster series. *J. Magn. Magn. Mater.* **2018**, *451*, 32–37.
- (16) Ding, X.-L.; Xue, W.; Ma, Y.-P.; Wang, Z.-C.; He, S.-G. Density functional study on cage and noncage (Fe_2O_3)_n clusters. *J. Chem. Phys.* **2009**, *130*, 014303.

- (17) Kirilyuk, A.; Fielicke, A.; Demyk, K.; von Helden, G.; Meijer, G.; Rasing, T. Ferrimagnetic cage-like Fe_4O_6 cluster: Structure determination from infrared dissociation spectroscopy. *Phys. Rev. B: Condens. Matter Mater. Phys.* **2010**, *82*, 020405.
- (18) Logemann, R.; de Wijs, G. A.; Katsnelson, M. I.; Kirilyuk, A. Geometric, electronic, and magnetic structure of Fe_xO_y^+ clusters. *Phys. Rev. B: Condens. Matter Mater. Phys.* **2015**, *92*, 144427.
- (19) Erlebach, A.; Huhn, C.; Jana, R.; Sierka, M. Structure and magnetic properties of $(\text{Fe}_2\text{O}_3)_n$ clusters ($n = 1-5$). *Phys. Chem. Chem. Phys.* **2014**, *16*, 26421–26426.
- (20) Janssens, E.; Santambrogio, G.; Brümmer, M.; Wöste, L.; Lievens, P.; Sauer, J.; Meijer, G.; Asmis, K. R. Isomorphous substitution in bimetallic oxide clusters. *Phys. Rev. Lett.* **2006**, *96*, 233401.
- (21) Santambrogio, G.; Janssens, E.; Li, S.; Siebert, T.; Meijer, G.; Asmis, K. R.; Döbler, J.; Sierka, M.; Sauer, J. Identification of conical structures in small aluminum oxide clusters: Infrared spectroscopy of $(\text{Al}_2\text{O}_3)_{1-4}(\text{AlO})^+$. *J. Am. Chem. Soc.* **2008**, *130*, 15143–15149.
- (22) Brümmer, M.; Kaposta, C.; Santambrogio, G.; Asmis, K. R. Formation and photodepletion of cluster ion-messenger atom complexes in a cold ion trap: Infrared spectroscopy of VO^+ , VO_2^+ , and VO_3^+ . *J. Chem. Phys.* **2003**, *119*, 12700–12703.
- (23) Asmis, K. R.; Sauer, J. Mass-selective vibrational spectroscopy of vanadium oxide cluster ions. *Mass Spectrom. Rev.* **2007**, *26*, 542–562.
- (24) van Dijk, C. N.; Roy, D. R.; Fielicke, A.; Rasing, T.; Reber, A. C.; Khanna, S. N.; Kirilyuk, A. Structure investigation of Co_xO_y^+ ($x = 3-6$, $y = 3-8$) clusters by ir vibrational spectroscopy and dft calculations. *Eur. Phys. J. D* **2014**, *68*, 357.
- (25) Goebbert, D. J.; Meijer, G.; Asmis, K. R.; et al. 10 K ring electrode trap-tandem mass spectrometer for infrared spectroscopy of mass selected ions. *AIP Conf. Proc.* **2009**, *1104*, 22–29.
- (26) Oepts, D.; Van der Meer, A.; Van Amersfoort, P. The free-electron-laser user facility felix. *Infrared Phys. Technol.* **1995**, *36*, 297–308.
- (27) Ferrari, P.; Vanbuel, J.; Li, Y.; Liao, T.-W.; Janssens, E.; Lievens, P. In *Gas-Phase Synthesis of Nanoparticles*; Huttel, Y., Ed.; Wiley-VCH: 2017; pp 59–78.
- (28) Wang, Y.; Lv, J.; Zhu, L.; Ma, Y. Crystal structure prediction via particle-swarm optimization. *Phys. Rev. B: Condens. Matter Mater. Phys.* **2010**, *82*, 094116.
- (29) Balabanov, N. B.; Peterson, K. A. Systematically convergent basis sets for transition metals. I. All-electron correlation consistent basis sets for the 3d elements Sc-Zn. *J. Chem. Phys.* **2005**, *123*, 064107.
- (30) Dunning, T. H., Jr. Gaussian basis sets for use in correlated molecular calculations. I. The atoms boron through neon and hydrogen. *J. Chem. Phys.* **1989**, *90*, 1007–1023.
- (31) Lee, C.; Yang, W.; Parr, R. G. Development of the colle-salvetti correlation-energy formula into a functional of the electron density. *Phys. Rev. B: Condens. Matter Mater. Phys.* **1988**, *37*, 785–789.
- (32) Becke, A. D. Density-functional exchange-energy approximation with correct asymptotic behavior. *Phys. Rev. A: At, Mol, Opt. Phys.* **1988**, *38*, 3098–3100.
- (33) Becke, A. D. Density-functional thermochemistry. III. The role of exact exchange. *J. Chem. Phys.* **1993**, *98*, 5648–5652.
- (34) Perdew, J. P. Density-functional approximation for the correlation energy of the inhomogeneous electron gas. *Phys. Rev. B: Condens. Matter Mater. Phys.* **1986**, *33*, 8822–8824.
- (35) Tao, J.; Perdew, J. P.; Staroverov, V. N.; Scuseria, G. E. Climbing the density functional ladder: Nonempirical meta-generalized gradient approximation designed for molecules and solids. *Phys. Rev. Lett.* **2003**, *91*, 146401.
- (36) Zhao, Y.; Truhlar, D. G. A new local density functional for main-group thermochemistry, transition metal bonding, thermochemical kinetics, and noncovalent interactions. *J. Chem. Phys.* **2006**, *125*, 194101.
- (37) Frisch, M. J.; Trucks, G. W.; Schlegel, H. B.; Scuseria, G. E.; Robb, M. A.; Cheeseman, J. R.; Scalmani, G.; Barone, V.; Mennucci, B.; Petersson, G. A. et al. *Gaussian-09*, Revision E.01; Gaussian Inc.: Wallingford, CT, 2009.
- (38) Grimme, S.; Antony, J.; Ehrlich, S.; Krieg, H. A consistent and accurate ab initio parametrization of density functional dispersion correction (DFT-d) for the 94 elements H-Pu. *J. Chem. Phys.* **2010**, *132*, 154104.
- (39) Pham, L. N.; Nguyen, M. T. Another look at photoelectron spectra of the anion Cr_2O_2^- : Multireference characters and energetic degeneracy. *J. Chem. Theory Comput.* **2018**, *14*, 4833–4843.
- (40) Calvo, F.; Li, Y.; Kiawi, D. M.; Bakker, J. M.; Parneix, P.; Janssens, E. Nonlinear effects in infrared action spectroscopy of silicon and vanadium oxide clusters: Experiment and kinetic modeling. *Phys. Chem. Chem. Phys.* **2015**, *17*, 25956–25967.
- (41) Vancoillie, S.; Malmqvist, P. A.; Veryazov, V. Potential energy surface of the chromium dimer re-re-revisited with multiconfigurational perturbation theory. *J. Chem. Theory Comput.* **2016**, *12*, 1647–1655.
- (42) Simard, B.; Lebeault-Dorget, M.-A.; Marijnissen, A.; ter Meulen, J. J. Photoionization spectroscopy of dichromium and dimolybdenum: Ionization potentials and bond energies. *J. Chem. Phys.* **1998**, *108*, 9668–9674.
- (43) Paul, S.; Misra, A. Magnetic properties of Cr_2O_n^- clusters: A theoretical study. *J. Mol. Struct.: THEOCHEM* **2009**, *895*, 156–160.